Prevention of surface recombination by electrochemical tuning of TiO_2-passivated photocatalysts

Bingya Hou, Fatemeh Rezaeifar, Jing Qiu, Guangtong Zeng, Rehan Kapadia, and Stephen B. Cronin

Citation: Appl. Phys. Lett. **111**, 141603 (2017); doi: 10.1063/1.4997483
View online: http://dx.doi.org/10.1063/1.4997483
View Table of Contents: http://aip.scitation.org/toc/apl/111/14
Published by the American Institute of Physics

Prevention of surface recombination by electrochemical tuning of TiO_2-passivated photocatalysts

Bingya Hou,[1] Fatemeh Rezaeifar,[1] Jing Qiu,[2] Guangtong Zeng,[3] Rehan Kapadia,[1] and Stephen B. Cronin[1,3]
[1]*Department of Electrical Engineering, University of Southern California, Los Angeles, California 90089, USA*
[2]*Department of Material Science, University of Southern California, Los Angeles, California 90089, USA*
[3]*Department of Chemistry, University of Southern California, Los Angeles, California 90089, USA*

(Received 24 July 2017; accepted 17 September 2017; published online 3 October 2017)

We present a systematic study of photoluminescence (PL) spectroscopy of TiO_2-passivated GaAs as a function of electrochemical potential in an ionic liquid solution. We observe a 7X increase in the PL intensity as the GaAs transitions from accumulation to depletion due to the applied potential. We attribute this to the excellent control over the surface Fermi level enabled by the high capacitance of the electrochemical double layer and TiO_2. This allows us to control the surface carrier concentration and corresponding non-radiative recombination rate. In addition to photoluminescence (PL) spectroscopy, we also measured the capacitance-potential (i.e., *C-V*) characteristics of these samples, which indicate flat band potentials that are consistent with these regimes of ion accumulation observed in the photoluminescence measurements. We have also performed electrostatic simulations of these *C-V* characteristics, which provide a detailed and quantitative picture of the conduction and valence band profiles and charge distribution at the surface of the semiconductor. These simulations also enable us to determine the range of potentials over which the semiconductor surface experiences depletion, inversion, and accumulation of free carriers. Based on these simulations, we can calculate the Shockley-Read-Hall recombination rate and model the PL intensity as a function of voltage. We show that this approach allows us to explain our experimental data well. *Published by AIP Publishing.*
https://doi.org/10.1063/1.4997483

At typical photocatalytic semiconductor-liquid interfaces, there is usually considered to be an equilibrium between the Fermi energy in the semiconductor and the redox potential of the ions in solution. This gives rise to band bending and a built-in potential at the surface of the semiconductor, which causes separation of the photoexcited electron-holes pairs, when illuminated.[1] In the photocatalysis literature, these bands are often only sketched qualitatively, even though commercially available tools for rigorous modeling are commonly used for semiconductor devices. In addition, there are electrostatic charges trapped at the surface of most semiconductors that further shift this equilibrium. As such, it is difficult (if not impossible) to predict the position of the flat band potential at a given semiconductor-liquid interface without careful calibration to experiment. Capacitance-voltage measurements (i.e., Mott-Schottky measurements) are commonly used to determine the carrier type[2–5] and establish the position of the flat band potential at the semiconductor-liquid interface experimentally.[6] The flat band potential of TiO_2-passivated InP photocathodes has been measured by Lin *et al.* using the Mott-Schottky method, by performing a linear fit of the $1/C^2$-V data and extrapolating the voltage axis intercept.[7] Hu *et al.* also used this method to acquire the values of the built-in voltage produced in *n*-type GaAs nanowire/CH_3CN-$FeCp_2^{+/0}$ junctions and planar GaAs/CH_3CN-$FeCp_2^{+/0}$ junctions.[8]

In addition to modulating the band bending, as mentioned above, the ions in the solution can screen trap surface charges in the semiconductor, which typically gives rise to surface recombination and represents a major loss mechanism in semiconductor photocatalysis. Over the past few years, several research groups have utilized ionic liquids to passivate the surface states of semiconductors.[9,10] This approach has been used to mitigate the effects of surface depletion[2,11] and non-radiative surface recombination due to the dangling bonds and surface states in the semiconductor.[9] Arab *et al.* observed a 12-fold enhancement in the PL intensity in GaAs nanowires with no applied potential and an up to 42× increase in the PL intensity of GaAs nanosheets with AlGaAs passivation.[9,12] In monolayer MoS_2, both the photocurrent and PL intensity are enhanced by a factor of two to three by ionic liquid gating.[10]

In the work presented here, we measure direct evidence of the reduction of surface recombination in a photocatalytic semiconductor under applied electrochemical potentials. We correlate the onset of this PL enhancement with flat band potentials obtained by *C-V* Mott-Schottky measurements, which enables us to determine the range of electrochemical potentials over which the semiconductor undergoes depletion, inversion, and accumulation of free charge. Electrostatic modeling of the *C-V* characteristics using Technology Computer Aided Design (TCAD) Sentaurus provides a detailed picture of the band profiles and charge distributions under these applied electrochemical potentials. A detailed mechanism of this gate-induced modulation of the PL efficiency is developed, within the context of this electrostatic model.

TiO_2-passivated semiconductors have become an important new class of photocatalyst. Here, a thin layer of TiO_2 deposited by atomic layer deposition (ALD) is able to prevent photocorrosion of most known semiconductors without sacrificing photocatalytic performance.[13–21] This represents a major breakthrough in photocatalysis, which was previously relegated to electrochemically robust materials like metal oxides, which typically have poor carrier mobilities and lifetimes, as well as large bandgaps. For example, in the work presented here, we use commercially available GaAs with a mobility of $\mu = 250\,cm^2/V{\cdot}s$, as compared to TiO_2, which has typical carrier mobilities of $\mu = 1\,cm^2/V{\cdot}s$.[22] Furthermore, the carrier concentration of the GaAs is known and is highly uniform, which enables precise modeling of the band bending at the photocatalytic interface. Here, we use *p*-type (111) oriented GaAs substrates with doping concentrations of $5.2–7.7 \times 10^{17}\,cm^{-3}$. Back ohmic contacts were made to the *p*-GaAs by evaporating 5 nm thick Ti followed by 50 nm of Au. Atomic layer deposition (ALD) of 5 nm TiO_2 was performed at 250 °C on the *p*-GaAs wafers, using Tetrakis(dimethylamido) titanium(IV) (TDMAT) as the titanium source and water vapor as the oxygen source. The carrier gas during the deposition was argon with a flow rate of 90 sccm, and TDMAT is used for the second half-cycle. An insulated copper wire was attached to the back contact of the p-GaAs sample using silver paint, and the entire sample, excluding the TiO_2-passivated surface, was encased in epoxy to insulate it from the solution. The solution is a non-aqueous ionic liquid solution consisting of 0.1 M 1-ethyl-3-methylimidazolium tetrafluoroborate ([EMIM] $[BF_4]$) in acetonitrile. A three-terminal potentiostat (Gamry Reference 600) was used to maintain a potential between the TiO_2-passivated GaAs working electrode and the $Ag/AgNO_3$ reference electrode. The calibration of the $Ag/AgNO_3$ electrode is given in the supplementary material. Under certain potentials, photoluminescence spectra were taken using a spectrometer (Renishaw *inVia* Raman Microscope) with a water immersion lens covered by a 13 μm thick Teflon sheet (American Durafilm) to protect it from the acetonitrile solution, as illustrated in Fig. 1. Mott-Schottky measurements were also performed by the Gamry Reference 600 potentiostat.

Figure 2 shows the photoluminescence intensity of a TiO_2-passivated GaAs photocathode, measured using the configuration illustrated in Fig. 1. Here, we see an increase in the photoluminescence intensity for potentials below −0.5 V vs. normal hydrogen electrode (NHE), reaching a 7-fold increase around −1.5 V vs. NHE. The $1/C^2$-V plot shown in Fig. 2(b) indicates a flat band potential of −0.5 V vs. NHE. This increase in the PL intensity is caused by the accumulation of cations on the surface of the semiconductor. These cations screen the surface states in the GaAs that normally cause nonradiative recombination, thus increasing the PL intensity. The surface states in the GaAs are associated with native defects, e.g., arsenic vacancies, gallium vacancies, and antisite defects.[23] Based on the $1/C^2$ vs. V curve plotted in Fig. 2(b), we are able to determine the range of potentials over which we have inversion, depletion, and accumulation of free carriers in the semiconductor, as labeled in Fig. 2(a).

In order to model the C-V behavior of our semiconductor surface, we performed electrostatic simulations of this device using the TCAD Sentaurus software package, which solves Poisson's equation iteratively with the electron and hole continuity equations and provides the self-consistent charge density profile in the semiconductor. Here, we have used a *p*-type GaAs substrate and a 5 nm dielectric layer on top to model the device. We have included the effect of interface states on the C-V behavior by including interface traps at the semiconductor-dielectric (TiO_2) interface. The series capacitance of the TiO_2 layer plus the double layer is modeled by an effective dielectric constant of the TiO_2 layer. The voltage is applied to the back contact of the GaAs substrate, as in the experimental configuration. The simulated Mott-Schottky (i.e., $1/C^2$ vs. V) plot is shown in Fig. 2(d), which agrees well with the experimental data. By fitting the position and magnitude of the C–V plot, we can extract the band diagrams and charge distributions in the dark, as plotted in Fig. 3. For each of the figures [Figs. 3(a)–3(c)], the energy scale has been set relative to the Fermi Level. As such, in each figure, the 0 eV reference point corresponds to E_F. In this case, the significant difference in band diagrams between accumulation and inversion/depletion occurs because of the fundamentally

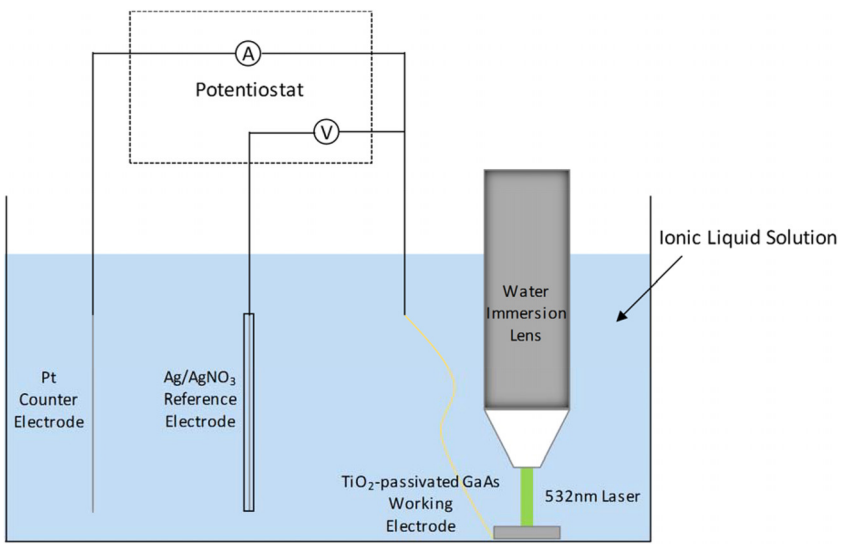

FIG. 1. Schematic diagram of the three-terminal photoelectrochemical cell. The water immersion lens is mounted on a microscope in the spectrometer for photoluminescence measurements.

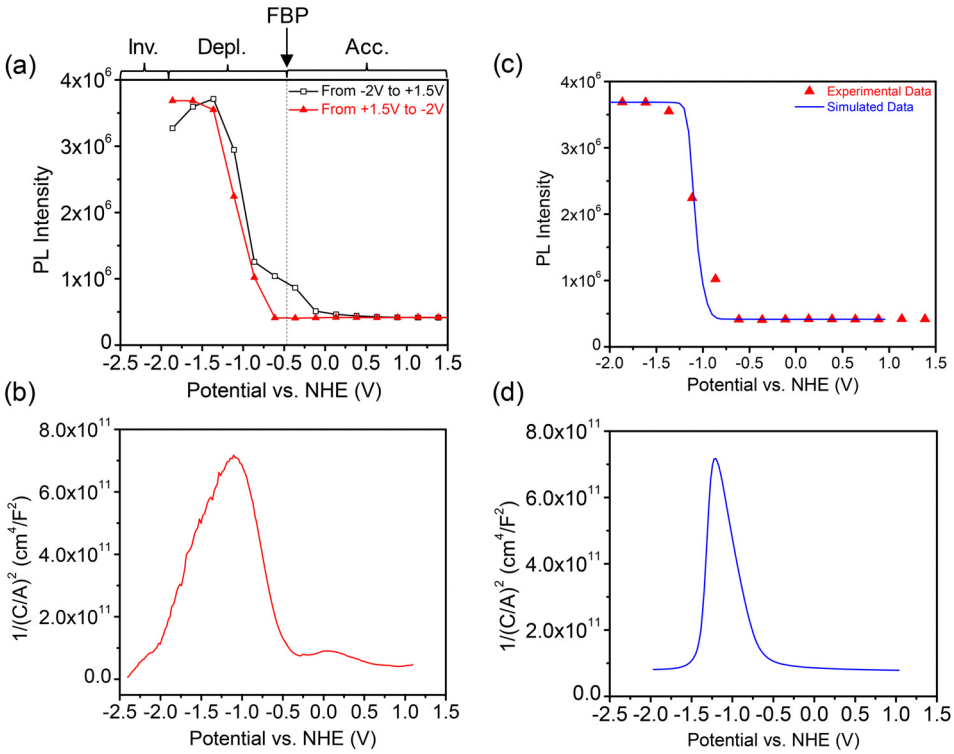

FIG. 2. (a) The photoluminescence intensity and (b) Mott-Schottky ($1/C^2$ vs. V) plot of a TiO_2-passivated GaAs photocathode measured as a function of the reference potential. [(c) and (d)] Simulated results for a GaAs photocathode over the same voltage range.

different physics that occurs at the surface. In p-GaAs, during depletion and inversion, an increased concentration of negative charge at the surface causes the surface Fermi level to move away from the valence band and closer to the conduction band. During accumulation, the increased concentration of positive charge at the surface causes the surface Fermi level to move in the opposite direction as compared to depletion/inversion.

The photoluminescence intensity in semiconductors can be written as the product of two terms, $(\text{Internal Radiative Efficiency}) \times (\text{Escape Probability})$, where the escape probability is the probability that a photon emitted in the semiconductor will escape into free space and is related to the geometry of the device and the carrier generation profiles. In our case, since the carrier generation profiles and geometry are fixed across the entire measurement range, we can assume that the change in luminescence efficiency can be modeled by a change in internal radiative efficiency. Thus, by tracking the filling fraction of these traps as a function of applied voltage, we can predict the change in radiative efficiency of our GaAs semiconductor by the following model:

$$Internal\ Radiative\ Efficiency = \frac{Bn^2}{An + Sn + Bn^2},$$

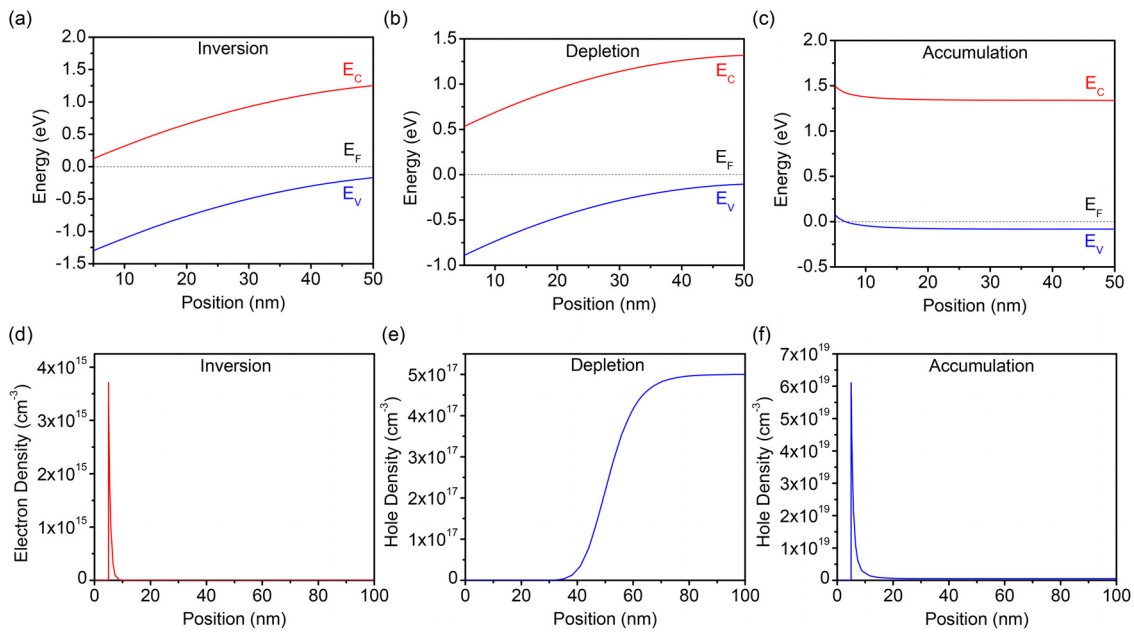

FIG. 3. Energy band diagrams and free carrier concentration of the semiconductor surface under (a) and (d) inversion, (b) and (e) depletion, and (c) and (f) accumulation conditions.

where A is the bulk Shockley-Read-Hall (SRH) recombination parameter, B is the radiative recombination parameter, S is a fitting parameter corresponding to SRH recombination due to the surface, and n is the carrier concentration. We have shown in Fig. 2 that we can quantitatively extract the position of the surface Fermi level in the dark through a combination of experimental measurements and simulations. We use this to calculate the change in the surface recombination parameter S as a function of applied voltage under optical illumination. To carry this out, we use the full equation for SRH recombination,[24]

$$U = \frac{\sigma_n \sigma_p v_{th} N_t \left(np - n_i^2\right)}{\sigma_n \left(n + n_i \exp\left(\frac{E_t - E_i}{kT}\right)\right) + \sigma_n \left(p + n_i \exp\left(\frac{E_i - E_t}{kT}\right)\right)},$$

where σ_n and σ_p are the electron and hole capture cross sections, v_{th} is the thermal velocity, N_t is the trap density, n and p are the electron and hole concentrations, n_i is the intrinsic carrier concentration, E_t is the trap energy level, and E_i is the intrinsic Fermi level. We can then evaluate this equation as a function of surface Fermi level and illumination. Here, we assume a trap distribution that exponentially decays in energy starting at the valence band edge, as previously measured for GaAs surfaces,[25] and integrate the recombination rate over the entire bandgap for each condition. To evaluate the carrier concentration as a function of band bending, we use the functions

$$n = Nc \exp\left(-\frac{E_C - E_F}{kT}\right) + \Delta n = Nc \exp\left(-\frac{E_C - E_{Fn}}{kT}\right),$$

$$p = Nv \exp\left(-\frac{E_F - E_V}{kT}\right) + \Delta p = Nv \exp\left(-\frac{E_{Fp} - E_V}{kT}\right),$$

to calculate the carrier concentration, where Nc and Nv are the effective density of states in the conduction and valence bands, and Δn and Δp are the excess carrier concentrations due to optical generation, which can be calculated by multiplying the optical generation rate by the carrier lifetime. E_F is the Fermi level of the system in the dark, and E_{Fn} and E_{Fp} are the electron and hole quasi-Fermi levels, respectively.

Figure 4(a) shows the normalized recombination rate plotted as a function of surface potential under light conditions. The details of the calculations, including the constants used, are given in the supplementary material. Here, we see that, when illuminated, the recombination rate peaks when the bands are flat (i.e., surface potential ~0 V) and when the bands are bent to near inversion (i.e., surface potential $\sim E_G/e$). This behavior can be understood by considering that the SRH recombination rate is dependent on the degree to which the semiconductor is out of equilibrium, quantified as np–n_i^2. Thus, when the surface is depleted, the primary source of electrons and holes will be optical generation. Since that rate is fixed by the external light source, the np product will remain fixed, and the recombination rate will remain fixed. However, when the surface is in the inversion or accumulation regions, the np product will increase, thus increasing the recombination rate. In our case, the recombination rate will

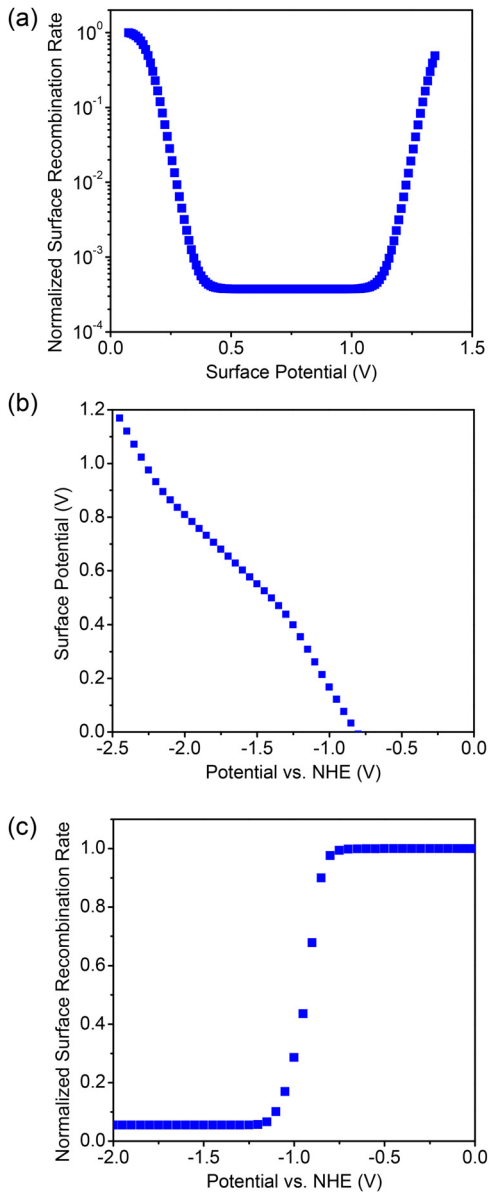

FIG. 4. (a) The normalized recombination rate of a GaAs semiconductor as a function of surface potential under illumination. (b) The surface potential plotted as a function of NHE extracted from the TCAD simulation. (c) The expected recombination rate as a function of applied bias under illumination.

increase when the electron or hole carrier concentration becomes large compared to the level set by optical generation. In order to model this behavior, we can use the optical generation rate in conjunction with the surface potential vs. NHE relation extracted from the TCAD simulation, as shown in Fig. 4(b), to calculate the expected recombination rate as a function of applied bias under illumination. With this, we obtain the relative change in the recombination rate near the surface, which we can then use as the parameter S to calculate the relative change in the internal radiative efficiency, which we have plotted in Fig. 2(c). Importantly, we see that this gives us good agreement with the experimental results.

The key physical reason behind the PL behavior exhibited here is the modulation of surface state recombination activity due to the relative location of the Fermi level in the bandgap. In both TiO_2-passivated GaAs and bare GaAs, there exists some distribution of surface states in the

bandgap. However, the specific energetic distributions and density may vary. Thus, this same overall behavior is expected from both bare and TiO_2-passivated surfaces. However, there will be differences in the magnitude of the effect, depending on both the distribution and density of surface traps.

Photocatalysis at the semiconductor-liquid interface represents a complex process, which includes band bending, built-in electric fields, surface recombination of photoexcited carriers, and charge transfer to the ions in solution. There are loss mechanisms associated with each of these key components to the overall photoconversion efficiency. This complex process is often oversimplified in order to provide a basic interpretation of the data. The method and results demonstrated here represent an important step towards obtaining a more rigorous understanding the overall "photocatalytic" or photoelectrochemical system, in which these key components can be decoupled experimentally.

In conclusion, we observe a large increase in the photoluminescence intensity under large negative applied potentials due to the electrochemically induced filling of surface states (i.e., surface recombination centers). GaAs, which is known to suffer from severe surface states, shows a 7× increase in photoluminescence intensity. By modeling the capacitance-voltage (i.e., $1/C^2$–V) data measured over the same range of applied electrochemical potentials, we obtain a detailed picture of the conduction and valence band profiles, as well as the charge density profiles, thus establishing the range of potentials over which the semiconductor undergoes depletion, inversion, and accumulation of free carriers. By calculating the relative surface recombination rates as a function of applied bias, we are able to accurately predict the modulation of the PL intensity that is observed experimentally.

See supplementary material for the details of the calculations of the normalized recombination rate as a function of surface potential under light conditions. The constants used are given in the supplementary material.

This research was supported by the Air Force Office of Scientific Research (AFOSR) Grant No. FA9550-15-1-0184 (B.H.), the Army Research Office (ARO) Award No. W911NF-14-1-0228 (J.Q.), the NSF Award No. CBET-1512505 (G.Z.), and the ACS-PRF Grant No. 55993-ND5 (R.K.).

[1]M. G. Walter, E. L. Warren, J. R. McKone, S. W. Boettcher, Q. Mi, E. A. Santori, and N. S. Lewis, "Solar water splitting cells," Chem. Rev. **110**, 6446–6473 (2010).
[2]J. W. Ager, R. E. Jones, D. M. Yamaguchi, K. M. Yu, W. Walukiewicz, S. X. Li, E. E. Haller, H. Lu, and W. J. Schaff, "p-type InN and In-rich InGaN," Phys. Status Solidi B **244**, 1820–1824 (2007).
[3]J. W. Ager, N. Miller, R. E. Jones, K. M. Yu, J. Wu, W. J. Schaff, and W. Walukiewicz, "Mg-doped InN and InGaN–photoluminescence, capacitance–voltage and thermopower measurements," Phys. Status Solidi B **245**, 873–877 (2008).
[4]K. Wang, N. Miller, R. Iwamoto, T. Yamaguchi, M. A. Mayer, T. Araki, Y. Nanishi, K. M. Yu, E. E. Haller, W. Walukiewicz, and J. W. Ager, "Mg doped InN and confirmation of free holes in InN," Appl. Phys. Lett. **98**, 042104 (2011).
[5]N. Miller, J. W. Ager, H. M. Smith, M. A. Mayer, K. M. Yu, E. E. Haller, W. Walukiewicz, W. J. Schaff, C. Gallinat, G. Koblmüller, and J. S. Speck, "Hole transport and photoluminescence in Mg-doped InN," J. Appl. Phys. **107**, 113712 (2010).
[6]N. Sato, *Electrochemistry at Metal and Semiconductor Electrodes* (Elsevier Science, 1998).
[7]Y. Lin, R. Kapadia, J. Yang, M. Zheng, K. Chen, M. Hettick, X. Yin, C. Battaglia, I. D. Sharp, J. W. Ager, and A. Javey, "Role of TiO_2 surface passivation on improving the performance of p-InP photocathodes," J. Phys. Chem. C **119**, 2308–2313 (2015).
[8]S. Hu, C.-Y. Chi, K. T. Fountaine, M. Yao, H. A. Atwater, P. D. Dapkus, N. S. Lewis, and C. Zhou, "Optical, electrical, and solar energy-conversion properties of gallium arsenide nanowire-array photoanodes," Energy Environ. Sci. **6**, 1879 (2013).
[9]S. Arab, P. D. Anderson, M. Yao, C. Zhou, P. D. Dapkus, M. L. Povinelli, and S. B. Cronin, "Enhanced Fabry-Perot resonance in GaAs nanowires through local field enhancement and surface passivation," Nano Res. **7**, 1146–1153 (2014).
[10]Z. Li, S.-W. Chang, C.-C. Chen, and S. B. Cronin, "Enhanced photocurrent and photoluminescence spectra in MoS_2 under ionic liquid gating," Nano Res. **7**, 973–980 (2014).
[11]G. F. Brown, J. W. Ager, W. Walukiewicz, W. J. Schaff, and J. Wu, "Probing and modulating surface electron accumulation in InN by the electrolyte gated hall effect," Appl. Phys. Lett. **93**, 262105 (2008).
[12]S. Arab, C. Chi, T. Shi, Y. Wang, D. P. Dapkus, H. E. Jackson, L. M. Smith, and S. B. Cronin, "Effects of surface passivation on twin-free GaAs nanosheets," ACS Nano **9**(2), 1336–1340 (2015).
[13]Y. W. Chen, J. D. Prange, S. Duhnen, Y. Park, M. Gunji, C. E. D. Chidsey, and P. C. McIntyre, "Atomic layer-deposited tunnel oxide stabilizes silicon photoanodes for water oxidation," Nat. Mater. **10**, 539–544 (2011).
[14]J. Qiu, G. Zeng, P. Pavaskar, Z. Li, and S. B. Cronin, "Plasmon-enhanced water splitting on TiO_2-passivated GaP photocatalysts," Phys. Chem. Chem. Phys. **16**, 3115 (2014).
[15]G. Zeng, J. Qiu, P. Pavaskar, Z. Li, and S. B. Cronin, "CO_2 reduction to methanol on TiO_2-passivated GaP photocatalysts," ACS Catal. **4**, 3512 (2014).
[16]M. H. Lee, K. Takei, J. J. Zhang, R. Kapadia, M. Zheng, Y. Z. Chen, J. Nah, T. S. Matthews, Y. L. Chueh, J. W. Ager, and A. Javey, "p-type InP nanopillar photocathodes for efficient solar-driven hydrogen production," Angew. Chem. Int. Ed. **51**, 10760 (2012).
[17]S. Hu, M. R. Shaner, J. A. Beardslee, M. Lichterman, B. S. Brunschwig, and N. S. Lewis, "Amorphous TiO_2 coatings stabilize Si, GaAs, and GaP photoanodes for efficient water oxidation," Science **344**, 1005–1009 (2014).
[18]J. Qiu, G. T. Zeng, M. Y. Ge, S. Arab, M. Mecklenburg, B. Y. Hou, C. F. Shen, A. V. Benderskii, and S. B. Cronin, "Correlation of Ti^{3+} states with photocatalytic enhancement in TiO_2-passivated p-GaAs," J. Catal. **337**, 133–137 (2016).
[19]J. Qiu, G. Zeng, M. Ge, Y. Lin, A. Javey, and S. B. Cronin, "Artificial photosynthesis on TiO_2-passivated InP nanopillars," Nano Lett. **15**(9), 6177–6181 (2015).
[20]J. Qiu, G. T. Zeng, M. A. Ha, B. Y. Hou, M. Mecklenburg, H. T. Shi, A. N. Alexandrova, and S. B. Cronin, "Microscopic study of atomic layer deposition of TiO_2 on GaAs and its photocatalytic application," Chem. Mater. **27**, 7977–7981 (2015).
[21]G. T. Zeng, J. Qiu, B. Y. Hou, H. T. Shi, Y. J. Lin, M. Hettick, A. Javey, and S. B. Cronin, "Enhanced photocatalytic reduction of CO_2 to CO through TiO_2 passivation of InP in ionic liquids," Chemistry **21**, 13502 (2015).
[22]P. Tiwani, P. Docampo, M. B. Johnston, H. J. Snaith, and L. M. Herz, "Electron mobility and injection dynamics in mesoporous ZnO, SnO_2, and TiO_2 films used in dye-sensitized solar cells," ACS Nano **5**, 5158–5166 (2011).
[23]J. M. Woodall and J. L. Freeouf, "GaAs metallization: Some problems and trends," J. Vac. Sci. Technol. **19**, 794–798 (1981).
[24]S. Sze, *Physics of Semiconductor Devices*, 3rd ed. (Wiley, 2006).
[25]M. Passlack, M. Hong, and J. P. Mannaerts, "Quasistatic and high frequency capacitance–voltage characterization of Ga_2O_3–GaAs structures fabricated by in situ molecular beam epitaxy," Appl. Phys. Lett. **68**, 1099–1101 (1996).